Molecular Microbiology (2019) 111(6), 1689–1699

doi:10.1111/mmi.14246
First published online 17 April 2019

Sodium-powered stators of the bacterial flagellar motor can generate torque in the presence of phenamil with mutations near the peptidoglycan-binding region

Tsubasa Ishida,[1†] Rie Ito,[1†] Jessica Clark,[2] Nicholas J. Matzke,[3] Yoshiyuki Sowa[1,4‡] and Matthew A. B. Baker [2*‡]

[1] *Department of Frontier Bioscience, Hosei University, Tokyo, Japan.*
[2] *School of Biotechnology and Biomolecular Science, University of New South Wales, Kensington, NSW Australia.*
[3] *School of Biological Sciences, University of Auckland, Auckland, New Zealand.*
[4] *Research Center for Micro-Nano Technology, Hosei University, Tokyo, Japan.*

Summary

The bacterial flagellar motor powers the rotation that propels the swimming bacteria. Rotational torque is generated by harnessing the flow of ions through ion channels known as stators which couple the energy from the ion gradient across the inner membrane to rotation of the rotor. Here, we used error-prone PCR to introduce single point mutations into the sodium-powered *Vibrio alginolyticus*/*Escherichia coli* chimeric stator PotB and selected for motors that exhibited motility in the presence of the sodium-channel inhibitor phenamil. We found single mutations that enable motility under phenamil occurred at two sites: (i) the transmembrane domain of PotB, corresponding to the TM region of the PomB stator from *V. alginolyticus* and (ii) near the peptidoglycan binding region that corresponds to the C-terminal region of the MotB stator from *E. coli.* Single cell rotation assays confirmed that individual flagellar motors could rotate in up to 100 μM phenamil. Using phylogenetic logistic regression, we found correlation between natural residue variation and ion source at positions corresponding to PotB F22Y, but not at other sites. Our results demonstrate that it is not only the pore region of the stator that moderates motility in the presence of ion-channel blockers.

Accepted 15 March, 2019. *For correspondence. E-mail matthew.baker@unsw.edu.au; Tel. +61 2 9385 1255; Fax: +61 2 9385 1483.
†Equal contribution.
‡Joint corresponding authors.

Introduction

Motility imparts a large benefit to organisms competing for sparse nutrients. The bacterial flagellum is the oldest known form of motility (Rossmann and Beeby, 2018), consisting of a propeller-like filament that rotates under the power of the bacterial flagellar motor (BFM). The BFM is 40 nm in diameter, powered by ion transit across the cell membrane through the stator protein complex, a heterodimer which forms a selective ion channel that transduces chemical energy into mechanical torque (Minamino *et al.*, 2018). While most stators are proton-powered (Sowa and Berry, 2008), some from marine habitats are sodium-powered (Yorimitsu and Homma, 2001), others are powered by both sodium ions and protons (Paulick *et al.*, 2015), and recently some have been discovered that they are even powered by large divalent cations (Imazawa *et al.*, 2016). In general, flagellar motors have adapted to function in various environments where bacteria live and survive (Terashima *et al.*, 2017; Chaban *et al.*, 2018; Rossmann and Beeby, 2018). BFM diversity creates an ideal case study to investigate how macromolecular complexes adapt to different environments.

In *Escherichia coli*, the energy from the proton gradient is harnessed by the transit of protons through a heterodimeric stator complex of a homotetramer and a homodimer ($MotA_4MotB_2$) (Minamino *et al.*, 2018). In *Vibrio* species this heterodimer is the sodium ion-powered $PomA_4PomB_2$. The total complex, in both cases, consists of four transmembrane (TM) domains of the A-subunit, a single TM domain of the B-subunit and a large periplasmic region of the B-subunit which consists of a plug segment and a peptidoglycan-binding (PG-binding) region (Kojima and Blair, 2001; Kojima *et al.*, 2009). Recently, the structural rearrangements in PG-binding and stator activation

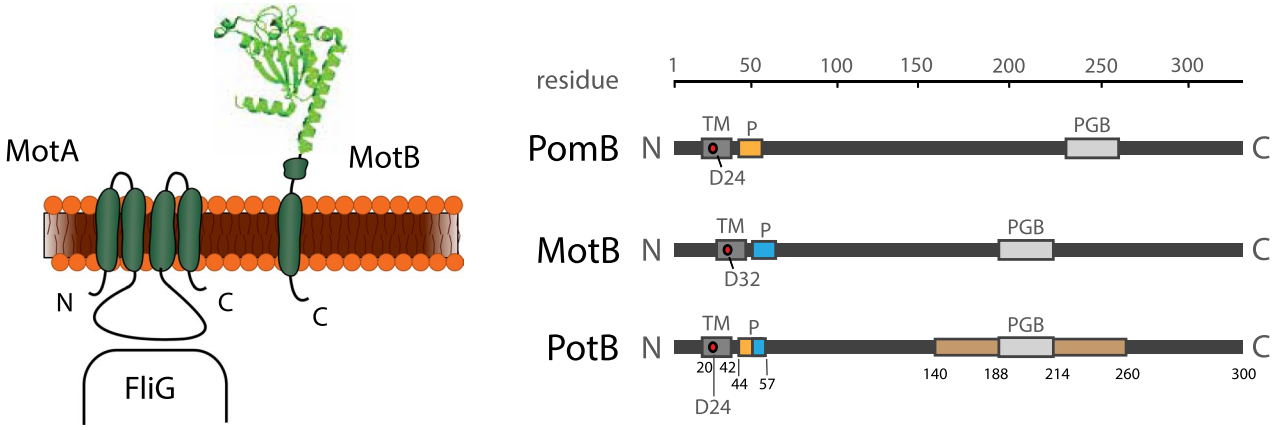

Fig. 1. Schematic and structure of the stators of the bacterial flagellar motor.
A. The stator complex in *E. coli* consists of a heterodimeric complex composed of $MotA_4MotB_2$. Each stator has two ion channels that are composed of four TM domains of MotA and one TM domain of MotB.
B. The PotB chimera consists of residues 1–50 from *V. alginolyticus* PomA and residues 59–308 of *E. coli* MotB with TM, plug, PGB and ompA-like regions (brown bar) indicated on the schematic respectively. Structure in A from Kojima *et al.* (2008). [Colour figure can be viewed at wileyonlinelibrary.com]

were resolved, indicating that conformational rearrangements of the linker between the PG-binding region and the TM-domain are critical in stator activation (Kojima *et al.*, 2018).

Whilst crystal structures have been solved for the C-terminal domains of MotB in multiple species (Roujeinikova, 2008; Kojima *et al.*, 2009; Zhu *et al.*, 2014), the full structure of the TM-domain in any species has yet to be resolved beyond the low-resolution of cryoEM of the entire stator complex (Yonekura *et al.*, 2011). Much of our understanding of stator function in the TM-domain relies on mutagenesis (Sharp *et al.*, 1995; Yakushi *et al.*, 2006). Chimeric B-subunits have been engineered that combine the C-terminal peptidoglycan binding motif of the MotB subunit with the transmembrane domain of PomB to form the ion channel (in complex with two subunits of PomA) (Asai *et al.*, 2003) (Fig. 1). These chimeric $PomA_4PotB_2$ stators utilise the sodium-motive force (SMF) to drive flagellar rotation and can bind to the peptidoglycan (PG) layer, thus enabling *E. coli* to swim under SMF. They have enabled the function of the motor to be investigated at low sodium concentration, and thus low energisation (Sowa *et al.*, 2005; Lo *et al.*, 2013).

Since this chimeric stator complex is driven by sodium ion flow across the inner membrane, it is natural to examine how sodium channel blockers affect this process. Phenamil, a known sodium channel blocker (Garvin *et al.*, 1985), has been used to probe sodium-interaction sites in sodium-driven motors *in situ* in *Vibrio* species (Sugiyama *et al.*, 1988; Atsumi *et al.*, 1990). Work in *Vibrio alginolyticus* demonstrated that the motility under phenamil could be restored by mutations at the cytoplasmic end of the TM-domain of the stator complex (Kojima *et al.*, 1997; 1999). *Vibrio parahaemolyticus* has been widely studied as a model for dual-powered motility; it has lateral flagella that are proton powered but polar flagella that are sodium-powered (Atsumi *et al.*, 1992). Directed evolution approaches have been applied to *V. parahaemolyticus* to examine which spontaneous mutations might induce resistance to phenamil (Jaques *et al.*, 1999). Jaques *et al.* selected for resistance to phenamil by selecting flagellar motors that were motile in the presence of 40 μM phenamil methanesulfonate, yet interestingly only observed a single mutant in the TM-domain that resulted in phenamil resistance.

Here, we engineered a plasmid construct with enzyme cut sites adjacent to PotB to examine the effects of randomly generated mutations on motility. We screened using phenamil to measure the frequency and location of mutations that enabled motility under phenamil in the sodium-powered $PomA_4PotB_2$ chimera. We induced mutations at a controllable rate using error-prone PCR (error-prone PCR) and screened large populations of cells using streaking of transformed error-prone PCR product onto swim agar in streaks for screening and subsequent sequencing. This allowed a high-throughput screen to determine which mutations have resulted in strains that were functional in the presence of phenamil. We examined how frequently these mutations arose naturally using phylogenetics and parsimony reconstruction to determine whether these adaptations were correlated with existing PomB/MotB classification. By examining the structural and sequence location of these mutations, we have assembled a model that outlines the relationship between PG-binding and stator activity, and presented a framework for determining which residues hold evolutionary importance and may constrain the possible adaptive pathways available to the stators.

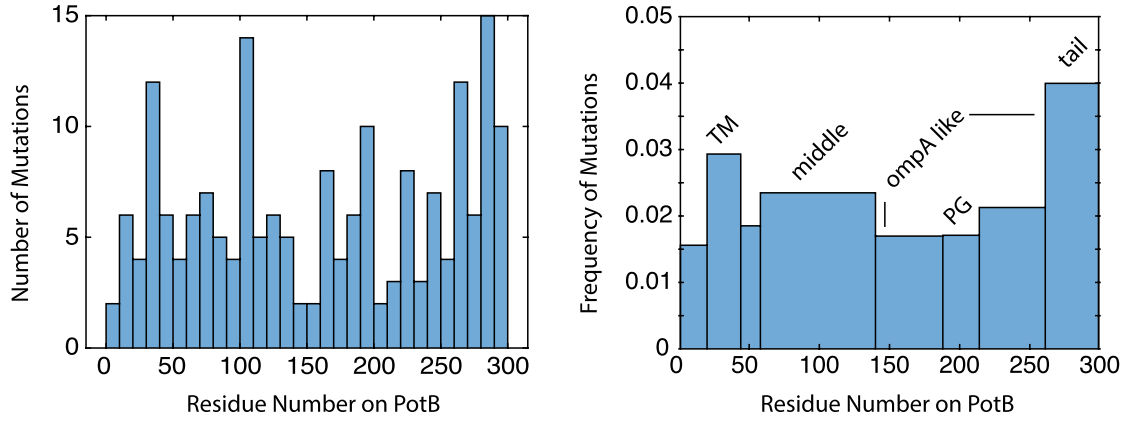

Fig. 2. Histogram of mutant frequency. Histograms of mutations from error-prone PCR across every strain with at least partial motility in phenamil (from spread plate).
A. Binned evenly across PotB with each bin 10 residues in width showing raw counts of mutations across aggregated results from all 27 error-prone PCR plasmids.
B. Frequency of mutations binned according to specific regions of PotB: TM (20–42), plug (44–57), middle (58–139), ompA-like first section (140–187), PG region (188–214), ompA-like second section (215–260) and tail (261–300). Counts are normalised across each region and strain (average mutations per residue per strain), and the mean across the entire protein is indicated by the dashed red line (0.026 mutations per residue per strain). [Colour figure can be viewed at wileyonlinelibrary.com]

Results

Mutagenesis of PotB

We generated mutations across the entirety of the PotB protein using error-prone PCR as per *Experimental procedures*. We defined the following regions across the PotB protein (numbering via PotB residue number): the TM domain (20–42), the plug (44–57), the middle domain (57–140), the ompA-like domain (140–260) and the peptidoglycan binding domain (188–214). We screened the combinatoric pool of mutagenesis outputs using swim streaking (Fig. S1) and characterised the motility of 27 error-prone PCR plasmids that exhibited some motility when selected for motility in the presence of phenamil (Fig. S2 and Table S1). The distribution of all nucleotide mutations in all 27 plasmids, including silent mutations, is shown in Fig. 2.

Together, these histograms indicated that the mutations occurred roughly evenly throughout the protein. We quantified the mutation rate in each region of the protein by calculating the mean number of mutations per strain in each region and normalising for the length of each region to calculate a mutation rate per residue for each region (Fig. 2B). We observed that proportionately more mutations occurred in the TM and the tail region of PotB, that is, the mutation rate was 0.031 and 0.044 mutations/residue in the TM and tail region, respectively, which was greater than the overall mutation rate across the entire protein, which was 0.026 mutations/residue.

Point mutations in TM domain can enable motility in the presence of phenamil

Out of 27 strains (Table S1), 209 mutations were observed in total, with a median number of mutations per strain of 8. Of the 209 nucleotide mutations, 62 were silent mutations that did not result in an amino acid change. Six exhibited a strong motility phenotype when motility was characterised in the presence of 20 μM of phenamil. Of particular interest, we focused on plasmid PotB-ep18 (Figs. S1-S2 and Table S1) which contained only three mutations: F22Y, L28Q and K100Q, and demonstrated increased motility in the presence of phenamil. To address the relative contributions of each mutation to the observed phenotype, we synthesised single point mutants of each of the three mutations (Fig. S3). Both F22Y and L28Q alone enabled motility under phenamil to PotB (Fig. 3), or together (pSHU149 and F22Y/L28Q), where they were slightly additive. Mutation K100Q appeared to offer no benefit in motility under phenamil, and as such was classified a redundant mutation. These results indicate that single point mutations, particularly in the pore region of the TM domain of PotB, can enable motility under phenamil.

Point mutations near PG-binding domain enable motility in the presence of phenamil

Plasmid PotB-ep9 (Figs. S1-S2 and Table S1) displayed a phenamil-resistant phenotype and also had only three

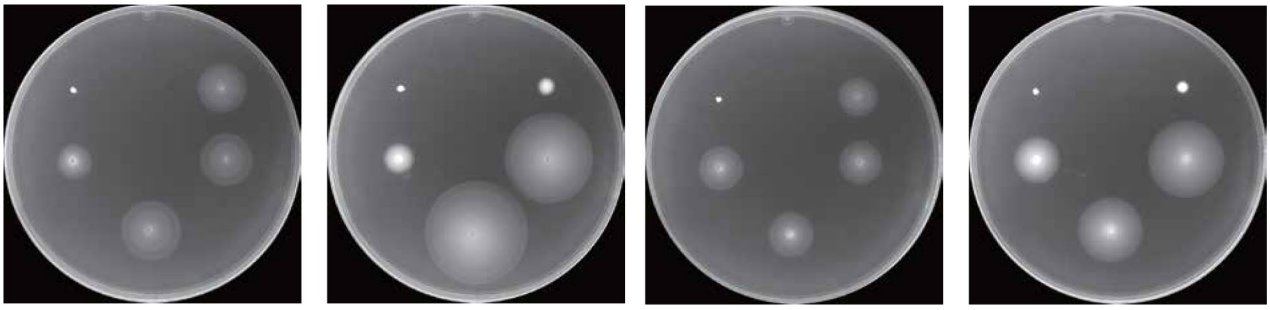

Fig. 3. Mutants in TM-domain and PG-binding region enable motility under phenamil. Motility of either TM-domain mutants (A/B) or PG-binding mutants (C/D) was tested via 0.25% agar swim plating using the empty vector (pBAD33) and PomAPotB wild-type as a negative and positive control respectively. A/C. In the absence of phenamil, swimming of mutants is comparable to the positive control. B/D. In the presence of 20 μM of phenamil, the mutants are motile whilst PomAPotB wild-type is severely limited. A/C incubated at 30°C for 10 h, B/D incubated at 30°C for 18 h. [Colour figure can be viewed at wileyonlinelibrary.com]

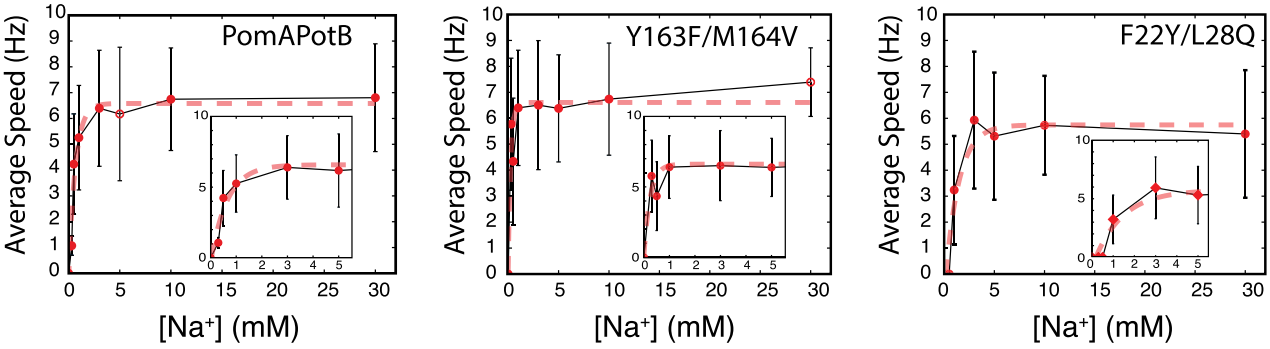

Fig. 4. Y163F/M164V is motile at less than 0.3 mM of [NaCl].
A. The PomAPotB wild-type exhibits single cell rotation from 0.3 mM of Na^+, increasing exponentially to a plateau above 6 Hz at full energisation.
B. PotB Y163F/M164V displays rotation at 0.3 mM of Na^+, with plateau above 6 Hz at full energisation.
C. potB F22Y/L28Q displays no rotation below 1 mM of Na^+, with a slower increase to a lower maximum speed plateau above 5 Hz and under 6 Hz. Inset in ABC shows zoom around 0–5 mM of [Na^+]. Dashed lines indicate monoexponential fit ($\omega = ae^{-bx} + c$). [Colour figure can be viewed at wileyonlinelibrary.com]

mutations: Y163F, M164V and L255M. This was targeted for further investigation as these mutations were all far from the TM domain. We again characterised the contributions of each mutation to motility and observed that Y163F and M164V each separately enabled motility in the presence of phenamil and that L255M was a redundant mutation (Fig. S3). When both mutations were combined in a single plasmid (pSHU146), motility in the presence of phenamil was increased (Fig. 3).

PG-binding double mutants rotate at lower sodium concentration than wild-type PotB

To establish whether these mutants were generating torque from sodium motive force, or had undergone a change in ion-specificity, we tested swimming in minimal sodium-free media (Fig. S4). None of the mutants were motile in sodium-free media, yet all plasmids restored swimming in the presence of sodium and in the presence and absence of phenamil (Fig S4). We then tested individual cells for rotation whilst lowering the concentration of sodium to determine whether the dependence on SMF had changed in these mutants (Fig. 4). This allowed us to confirm that our observed swim plate phenotype was caused changes in flagellar rotation, and account for any compensatory changes in growth or chemotaxis that might confound swim plate measurements. We examined the capacity of 'wild-type' PomAPotB (expressed via our plasmid pSHU1234, Fig. S5) and our mutant plasmids to restore swimming in 'sticky-filament' strains. These sticky-filament mutants lack the surface of the protein FliC, and thus undergo hydrophobic interactions with glass that enable filaments to stick to glass and allow the rotation of the body to be assessed in parallel (Kuwajima, 1988). In comparison with PomAPotB wild-type, the mutants in

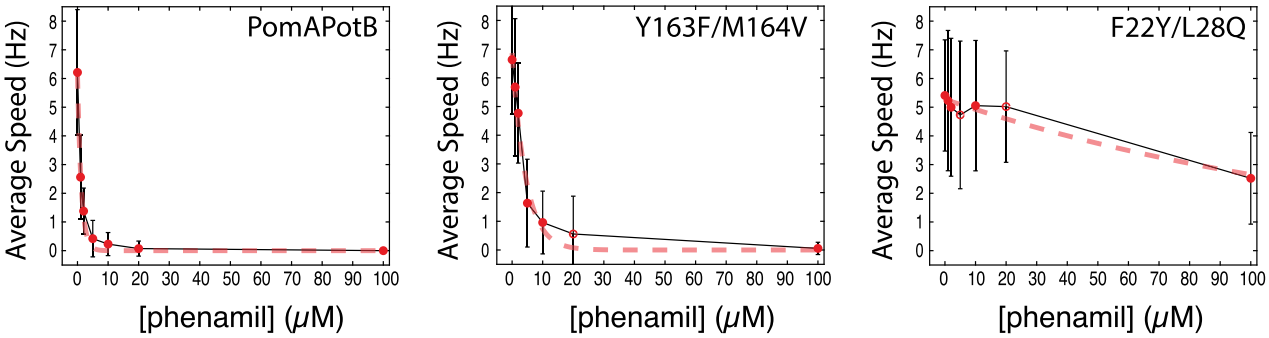

Fig. 5. TM mutants enable motility in phenamil concentrations up to 100 μM. Dose response of averaged measurements of single-cell rotation speed with varying concentration of phenamil for: (A) PomAPotB wild-type, (B) double TM-domain mutant (PomAPotB F22Y/L28Q) and (C) double PG-binding mutant (PomAPotB Y163F/M164V). Tethered cell data is fit with monoexponential decay curve to generate time constants for decay (PomAPotB wild-type: 0.8 mM^{-1}; PomAPotB Y163F/M164V: 0.2 mM^{-1}; PomAPotB F22Y/L28Q: 0.007 mM^{-1}). [Colour figure can be viewed at wileyonlinelibrary.com]

the PG-region (pSHU146: Y163F/M164V) were highly motile at low sodium (further detail Fig. S6), with cells rotating > 6 Hz in the presence of only 0.3 mM Na^+. This is in contrast to PomAPotB wild-type restoring motility to < 2 Hz at the equivalent SMF. In an opposite trend, mutations in the TM region (pSHU149: F22Y/L28Q) did not demonstrate swimming below 1 mM Na^+ and had a lower maximum speed and slower response to increased [Na^+].

TM-domain double mutants are not affected by increasing concentrations of phenamil

The response of single-cell speed with varying phenamil concentration was measured to examine the energy profile and structural basis of motility under phenamil in our two phenamil-resistant plasmids. In wild-type PomAPotB tethered cell rotation speed was reduced significantly when as little as 1 μM of phenamil was introduced, and cell speed plateaued at 5 μM of phenamil. The PG-binding double mutant (Y163F/M164V) demonstrated the same plateau effect in response to increasing phenamil but the concentration dependence of the decrease in rotational speed was much lower, that is, the decay constants for a monoexponential fit (fitting for b in: $\omega = ae^{-bx}$) were 0.8 and 0.2 mM^{-1} for PomAPotB wild-type and Y163F/M164V respectively. Similarly, the I_{50}, the concentrations of phenamil at which the speed was half the maximum, was 0.9 and 3.1 μM for wild-type and Y163F/M164V respectively. In contrast, the speed of rotation for the double TM-domain mutant (F22Y/L28Q) exhibited no dependence on phenamil concentration up to 20 μM, and only a 46% reduction on maximum speed at 100 μM phenamil. This implies that the mechanism of resistance in the TM-domain mutants destroyed much of the efficacy of phenamil to inhibit motility altogether, whereas the PG-binding region mutants acted to stabilise rotation in the presence of phenamil, but this stabilisation could be overcome as phenamil concentration was increased.

F22Y is common and clusters in phylogenies along MotB/PomB lines; L28Q is very rare

To explore the natural frequency of these residues and their correlation with ion specificity and motility outside the lab, a large low-level phylogeny of 948 MotB homologues was assembled which clearly divided into clades (Fig. 6A). We curated a subset of 34 commonly studied species where information on ion specificity exists in the literature (Fig. 6B–D). For each column of the subset alignment, we reconstructed ancestral residues with parsimony. At the F22Y site, residues clustered according to MotB/PomB identity (Fig. 6B), which is putatively linked to proton/sodium motility. To test if the correlation is greater than expected by chance, we used generalised linear models to perform phylogenetic and non-phylogenetic logistic regression (see *Experimental procedures*). This demonstrated that F/Y at position 22 had significant correlation with PomB/MotB respectively (Supporting Table S3). In contrast, at L28Q (Fig. 6D), the residue variation had no significant correlation with PomB/MotB. In fact, over the entire 948 species in the larger phylogeny, only one species had a glutamine at that site: *Myxococcus fulvus.*

Y163F/M164V are both rare and do not cluster along MotB/PomB lines

Similarly, we aligned the sequences in the section 156–214, including the PG-binding site, and measured correlation with PomB/MotB (Fig. 7 and Table 7). In both Y163F and M164V, logistic regression could not be run as these columns are not predominantly composed of

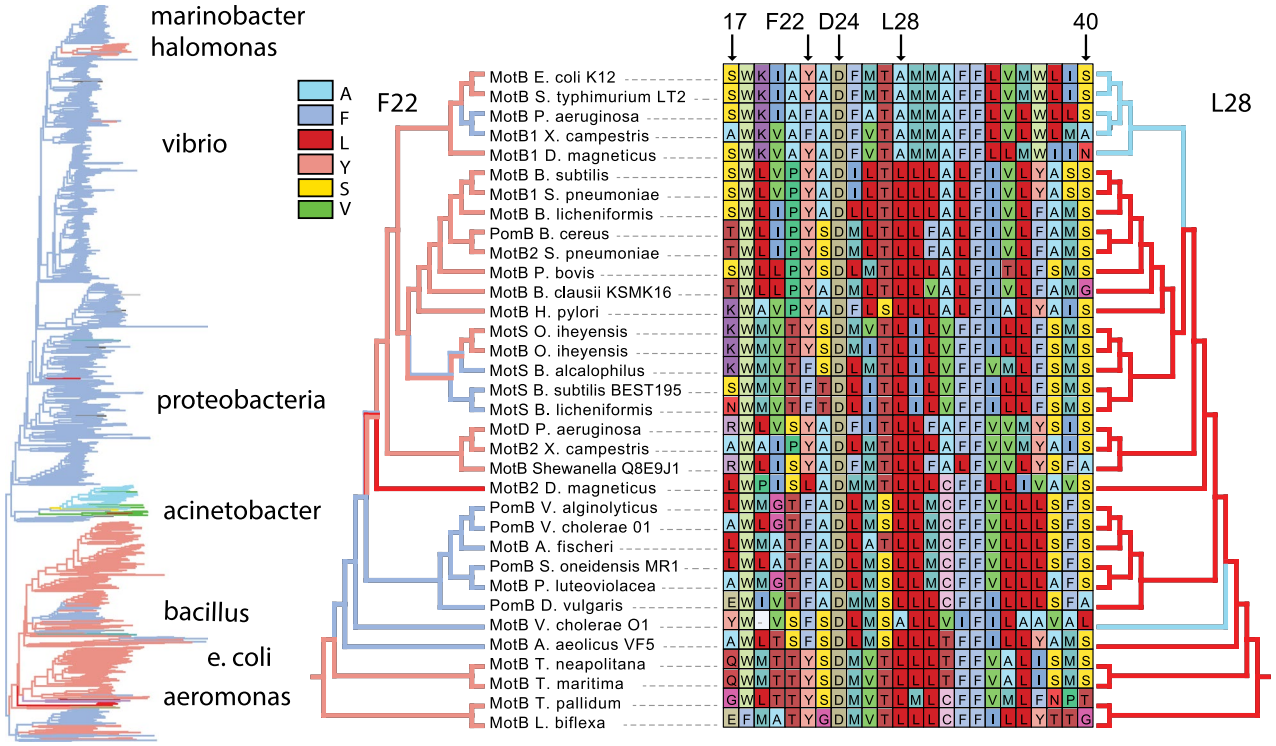

Fig. 6. Parsimony reconstruction for Y22 and L28.
A. Overall phylogeny of 948 MotB homologs coloured via sequence identity at site 22 showing clear signal (well-known clades are reproduced). Some major phyla indicated.
B. Parsimony reconstruction for site Y22 (PotB numbering) shown in colour over subset phylogeny of 34 representative species as labelled.
C. Sequence alignment across transmembrane domain of MotB/PomB showing conserved D24, and Y22/L28 mutations tested in this work.
D. Parsimony reconstruction for site L28A (PotB numbering) shown in colour over subset phylogeny. [Colour figure can be viewed at wileyonlinelibrary.com]

two residues (our algorithm requires a binary predictor variable). However, visual inspection suggests the mutations do not cluster along PomB/MotB lines. A phenylalanine at site 163 was very rare across the full phylogeny, occurring only in *Yersinia pestis biovar Orientalis.* The valine at site 163 was observed in 13 species, mostly among members of the *Spirochaetes* and *Oceanospirilla* families (Supporting Information Note).

Discussion

We have examined the effect of mutations in both the transmembrane domain and the peptidoglycan binding region of PotB to the binding of phenamil. Phenamil binding has been suggested to bind on the cytoplasmic face of the stator (Kojima *et al.*, 1997; 1999; Yakushi *et al.*, 2004), and function by limiting Na^+ exit into the cell interior (Yoshida *et al.*, 1990). However, the question remains how the mutations observed here, far from the pore, might influence phenamil binding and sodium transit. We observed that single point mutations in the TM region at L28 and F22 were sufficient to enable motility under phenamil. The mutation at F22Y is highly clustered around Pom/Mot stator subunits in varying species and presumably linked to sodium/proton specificity, which may show that residue F22 not only plays a role in sodium binding but also phenamil-binding and sodium blocking. Together with a mutation we observed as an error-prone PCR product at L28Q, these two mutations here have enabled motility under phenamil across a large range of phenamil concentrations, with stators remaining functional at concentrations of phenamil as high as 100 μM of phenamil. This high tolerance to phenamil implies that they have affected or removed the binding site of phenamil inside the pore region of the stator complex.

Previous work in *V. Alginolyticus* extensively explored the effect of mutations at PomB site 22 on motility in the presence and absence of phenamil (Terauchi *et al.*, 2011). Of these point mutations in PomB (as opposed to chimeric PotB), the substitutions F22S, F22W and F22N provided high motility under phenamil, however, it was also observed that F22Y displayed a phenotype of motility under phenamil. Our results confirm the importance of F22 site in the chimeric PotB and likely proximity to the Na^+ binding site and involvement in the ion-conducting

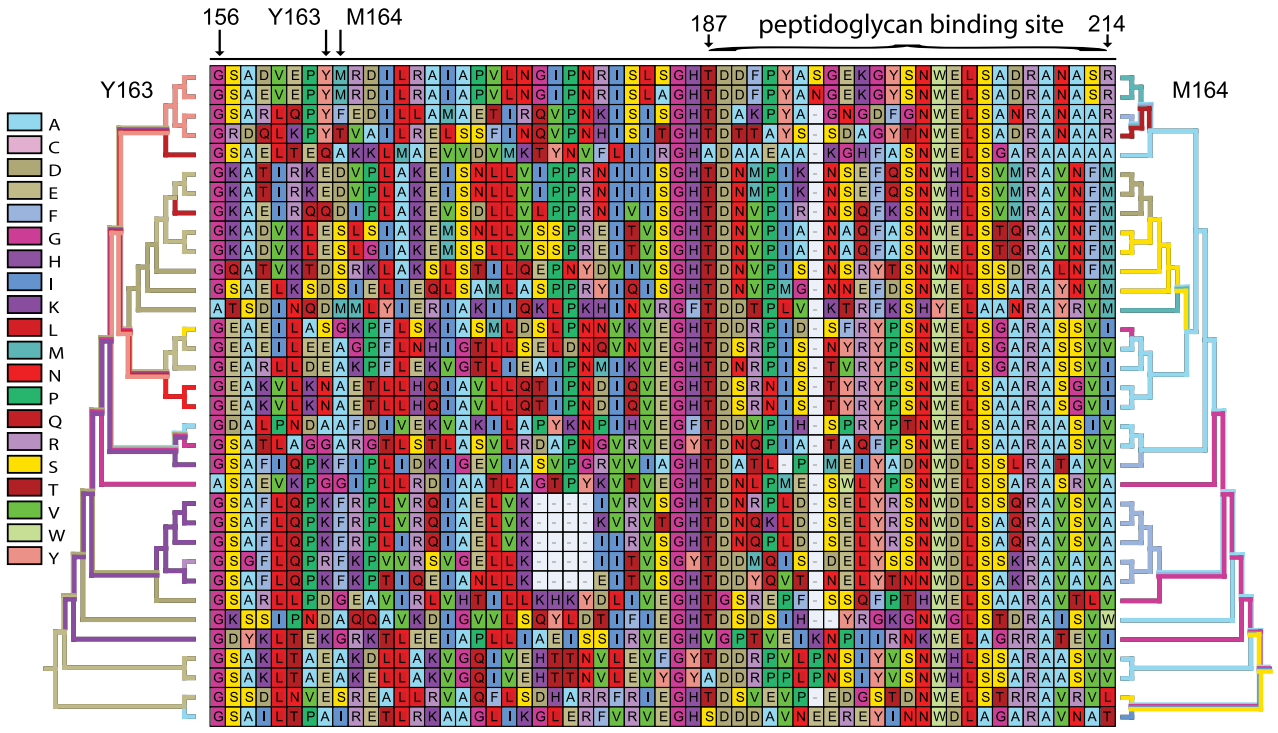

Fig. 7. Parsimony reconstruction for Y163 and M164.
A. Parsimony reconstruction for site Y163 (PotB numbering) shown in colour over subset phylogeny of 34 representative species from Fig. 5.
B. Sequence alignment over peptidoglycan binding site of MotB/PomB showing Y163/M164 mutations tested in this work.
C. Parsimony reconstruction for site M164 (PotB numbering) shown in colour over subset phylogeny. [Colour figure can be viewed at wileyonlinelibrary.com]

pathway, and show that even slight changes in the size of this residue can affect the binding site and enable motility under phenamil.

Similarly, in the PG-binding region we observed that two clustered single mutations were also sufficient to enable motility under phenamil. The PG-binding region is used to bind the stators in place so that they act on the motor. With these two mutations at Y163/M164 we observed a decaying concentration dependence of rotation to phenamil. These sites are far from the pore, which is expected to be the phenamil binding site. We consider that mutations near the PG region could allow motility under phenamil via two models: (i) changes to the PG region can impact stator-rotor interface and alter the pore region and phenamil binding site; and (ii) that changes to the PG region can alter the binding strength of PotB to the PG layer in *E. coli* and alter the dwell time of the stator on the rotor. The first option is supported by previous evidence that a mutation in the PG region of MotB (P159I) could be suppressed by a mutation on the rotor protein FliG (K192E) (Garza *et al.*, 1995). This suggested that changes in the PG region could influence the rotor-stator interface, and that this interface could be realigned with a compensatory mutation in the rotor. Thus, it is conceivable that our observed mutations in the PG region (Y163/M164) are influencing the rotor–stator interface, and thus altering the ion channel and the phenamil binding site, in a similar mechanism to change directly at the binding site caused by L28Q and F22Y. The second model contends that a change in the binding strength of the stator might increase the dwell time of the stator on the rotor is result in more stators being bound more often (Fig. 8). In turn, if each stator is fractionally functional, or occasionally able to pass a sodium ion in the presence of phenamil, then in total, with more stators on the rotor, these sodium-powered flagellar motors are able to function in the presence of phenamil. Recent structural evidence indicates that upon binding to the PG layer there is a dynamic rearrangement where a helix (helix α1) is extended into a non-helical structure to activates the stator and open the ion channel (Kojima *et al.*, 2018). Thus, it is also conceivable that mutations in the PG region could affect the release from the PG layer, the extension of helix α 1, or the conformational change that removes the plug from the channel. Further experiments are needed to distinguish between these models, for example, the use of single cell studies and single molecule fluorescence to measure changes in the dwell time of mutant stators on the motor, and tight regulation of

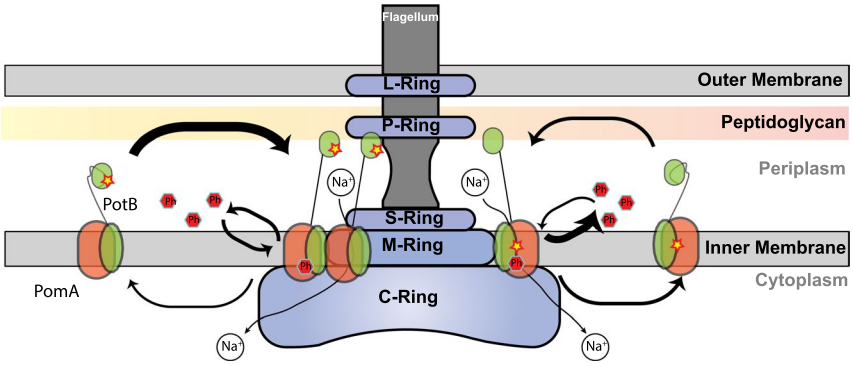

Fig. 8. Model of activity. Schematic showing effects of mutations with respect to phenamil and sodium flow through stator complex. The pool of stator complexes ($PomA_4PotB_2$) diffuse in the inner membrane, and when they bind to the motor the PG-binding region pulls with tension on the transmembrane domains of PomA and PotB (Kojima *et al.*, 2018). (left) Mutations in the 163/164 site affect PG-binding and the duration for which a stator is bound to the motor (dwell time). This could result in a slower off rate with respect to wild-type stators and a larger steady-state population of stators bound to the motor. In the presence of phenamil each stator has reduced functionality but in sum, with many stators, the motor is functional. (right) Mutations at the TM-domain near the putative phenamil binding site affect the binding and release of phenamil, thus phenamil is bound more weakly, and turns over more rapidly, allowing sodium ions to pass through the channel to generate motor rotation. An alternate possibility is that that mutations at 163/164 site cause a consequential alteration of the binding site, and thus limit phenamil binding in a similar manner to mutations at 22/28 site. [Colour figure can be viewed at wileyonlinelibrary.com]

stator expression to measure for dependence of motility on stator type, concentration and availability.

Phenamil resistance has been studied in other species, most notably in *V. parahaemolyticus*. This system is of interest as it has two motors, one sodium-powered and one proton-powered, and phenamil has been studied previously as a drug target for this pathogen (Atsumi *et al.*, 1992; Jaques *et al.*, 1999). Jaques *et al.* used natural selection over 12–18 days to screen for phenamil resistance (Jaques *et al.*, 1999). They observed a single mutation in the TM-domain, but did not observe the mutations that we saw in this paper. Their experiment, occurring through natural mutagenesis and evolution in a laboratory setting will respond to pleiotropy and epistasis and also inherent directionality in the process of stator adaptation. This means that the order of specific mutations can restrict the possible outcomes. Naturally, our mutation at L28Q was indeed very rare across our set of 948 MotB homologues, occurring only once in *M. fulvus* ~ 0.1% of the species we examined. Error-prone PCR however, is agnostic to the order of mutations and will insert mutations evenly across the protein of interest. This highlights the power of error-prone PCR to explore novel mutations and to compare historical evolutionary occurrences with those that can be discovered via directed and laboratory-assisted experimental evolution.

Our experimental system allows us to examine phenotypes to determine which amino acids have a functional cause in changing a phenotype. This allows us to address a common puzzle in phylogenetics because both mutations and traits are inherited on the phylogeny, in which they are non-independent, and can thus exhibit 'accidental' correlation without a functional relationship (Uyeda *et al.*, 2018). For example, in the case of MotB, every clade has some amino acids unique to it, but this will be true whether or not those residues have a functional role in the clade's motility phenotype. However, by characterising upmotile mutations in the presence of phenamil and adaptations in ion-source, we can directly test whether amino acid substitutions observed on the phylogeny are causally associated with a particular ion source, or a particular environment. This allows us to identify which amino acids, potentially in which order, have been part of historic adaptation events, such as a transition from sodium to proton-based motility. We can then use these approaches to tease out the causality of events that constrain natural adaptation.

Experimental procedures

Bacterial strains and plasmids

Bacterial strains and plasmids used in this study are listed in SI. For swim plating, plasmids were transformed into RP6665 (Δ*motAmotB*) (Block *et al.*, 1989) to restore motility. For tethered cell assays, plasmids were transformed into JHC36 (Δ*cheY fliC-sticky* Δ*pilA* Δ*motAmotB*) (Inoue *et al.*, 2008).

Error-prone PCR

Plasmid pSHU1234 was constructed in a pBAD33 backbone with unique cut-sites for NdeI and PstI directly upstream and downstream of PotB. Error-prone PCR was executed on pSHU1234 using primer 1176 and primer 0104 (Table S2), taq polymerase, unbalanced dNTPs and Mn^{2+}, as per (Wilson and Keefe, 2000). The post-PCR product and pSHU1234 was then digested and ligated with NdeI and PstI and transformed into RP6665 (Δ*motAB*).

Mutant isolation

Tranformant was streaked in lines on low agarose motility plate (Fig. S1) consisting of 0.25% TB soft agar (0.25% of bactoagar, 1% of bactotryptone and 0.5% of NaCl), 25 μg/mL of chloramphenicol, 1 mM of arabinose and 20 μM of phenamil. These plates were incubated at 30°C for 20 h. Flares were selected from these plates and single colonies were generated. These colonies were harvested, the plasmid was purified, transformed again into RP6665 and motility was tested as below. Specific mutants derived from error-prone PCR outcomes were engineered using a standard site-directed mutagenesis protocol with forward and reverse primers (Supporting Information), template and high-fidelity DNA polymerase (Pfu Ultra).

Motility assays

Motility testing was carried out using motility plate assays. Phenamil to a final concentration of either 0, 20 or 100 μM was added to the plates. Swim plates were inoculated from single colonies by toothpick. Plates were incubated for 10 or 18 h, respectively, as noted. For standard motility assays, plates consisted of minimal media for minimal motility assays (Fig. S4) consisted of 10 mM of KPO_4, 0.1% of glycerol, 0.1 mM of Thr, 0.1 mM of Leu, 0.1 mM of His, 0.1 mM of Met, 0.1 mM of Ser, 1 mM of $MgSO_4$, 1 mM of $(NH_2)_2SO_4$, 1 μg/mL of Thiamine and 0.5% of NaCl or KCl, respectively, (85 mM of [NaCl]; 67 mM of [KCl]), 1 mM of arabinose, 25 μg/mL of chloramphenicol and the indicated concentration of phenamil (0, 20 and 100 μM).

Sequence analysis

Sequencing was executed commercially by FASMAC (Japan) using forward and reverse primers and template (Table S2). Three primers were used to read the entire PomAPotB region.

Single cell speed assays

Cells were adhered spontaneously to glass coverslips via a sticky-filament and then imaged onto a CMOS camera at 60 frames per second thorough 40× objective. Rotation of tethered sticky-filament cells was analysed using custom software based upon LabView (National Instruments).

Phylogenetics and sequence diversity of MotB homologs

To survey the known flagellar diversity for amino acid substitutions similar to the upmotile mutations discovered by experiment, we estimated a very large phylogeny of MotB and related proteins. As our goal was exploratory, we chose faster heuristic methods feasible for a large data set, rather than Maximum Likelihood or Bayesian methods that would be impracticably slow. The 948 MotB homologs were assembled by searching the UniProt90 database against key study taxa. They were aligned using Clustal Omega (Larkin *et al*., 2007) on its most thorough settings (five iterations of re-alignment). The phylogeny was then estimated with Quicktree, a neighbour-joining method suitable for large data sets (Howe *et al*., 2002). The phylogeny was midpoint-rooted in FigTree (Rambaut 2018). As these are fast heuristic methods based on a single protein, deeper branches and rooting should be considered uncertain, and we make no claim about, for example, inter-phylum relationships, a very difficult phylogenetic problem (Pallen and Matzke, 2006; Abby and Rocha, 2012; Shih and Matzke, 2013; Koonin, 2016). However, the tree was adequate for the purpose of showing relationships between closer relatives, and for surveying MotB sequence conservation and diversity.

To further explore conservation and diversity at key positions of the alignment, ancestral amino acids were reconstructed on the phylogeny using parsimony in Mesquite (Maddison and Maddison, 2015). The 948-protein tree was subset to key study taxa for Figs. 6 and 7.

Logistic regression

We classified each species in the 34-species subset phylogeny as Na+, H+ or N/A to create a binary response variable for a logistic regression analysis. We were interested in cases where this binary response might be correlated with a binary amino acid predictor, so we filtered the columns of the subset alignment for columns where only two amino acids were predominantly observed. We excluded any column where the two most common amino acids added up to < 85% of the observed residues. We also excluded any site where the first or second most common amino acid had a < 10% frequency. These steps excluded the 163/164 site, but included positions 22/28. We ran two models to correlate each amino acid or the mutational pair with the ion source available: (i) non-phylogenetic logistic GLM (glm, R), and (ii) a phylogenetic logistic glm (phyloglm, R; Ives and Garland, 2010). We present the slope estimates, errors, and *z* scores and *P* values in Table S4, and our classification list of ionic energy sources in Table S5.

Acknowledgements

NJM was supported by ARC DECRA fellowship DE150101773 and Marsden grants 16-UOA-277 and 18-UOA-034. YS was supported by JSPS KAKENHI (18H02475 and 15K07034), MEXT KAKENHI (15H01332), Itoh Science Foundation and Casio Science Promotion Foundation. MABB was supported by the UNSW Scientia Research Fellowship, the CSIRO Synthetic Biology Future Science Platform 2018 Project Grant and ARC Discovery Project DP190100497.

Author contributions

TI collected and analysed the data. RI collected and analysed the data. JC collected the data. NJM analysed the data and wrote the manuscript. YS conceived and

supervised the project, collected and analysed the data, and wrote the manuscript. MABB conceived and supervised the project, collected and analysed the data, and wrote the manuscript.

References

Abby, S.S. and Rocha, E.P.C. (2012) The non-flagellar type III secretion system evolved from the bacterial flagellum and diversified into host-cell adapted systems. *PLOS Genetics*, **8**(9), e1002983. https://doi.org/10.1371/journal.pgen.1002983

Asai, Y., Yakushi, T., Kawagishi, I. and Homma, M. (2003) Ion-coupling determinants of Na+-driven and H+-driven flagellar motors. *Journal of Molecular Biology*, **327**(2), 453–463. https://doi.org/10.1016/S0022-2836(03)00096-2

Atsumi, T., Sugiyama, S., Cragoe, E.J. and Imae, Y. (1990) Specific inhibition of the Na(+)-driven flagellar motors of alkalophilic bacillus strains by the amiloride analog phenamil. *Journal of Bacteriology*, **172**(3), 1634–1639.

Atsumi, T., McCartert, L. and Imae, Y. (1992) Polar and lateral flagellar motors of marine vibrio are driven by different ion-motive forces. *Nature*, **355**(6356), 182–184. https://doi.org/10.1038/355182a0

Block, S.M., Blair, D.F. and Berg, H.C. (1989) Compliance of bacterial flagella measured with optical tweezers. *Nature*, **338**(6215), 514–518. https://doi.org/10.1038/338514a0

Chaban, B., Coleman, I. and Beeby, M. (2018) Evolution of higher torque in *Campylobacter*-type bacterial flagellar motors. *Scientific Reports*, **8**(1), 97. https://doi.org/10.1038/s41598-017-18115-1

Garvin, J.L., Simon, S.A., Cragoe, E.J. and Mandel, L.J. (1985) Phenamil: an irreversible inhibitor of sodium channels in the toad urinary bladder. *Journal of Membrane Biology*, **87**(1), 45–54.

Garza, A.G., Harris-Haller, L.W., Stoebner, R.A. and Manson, M.D. (1995) Motility protein interactions in the bacterial flagellar motor. *Proceedings of the National Academy of Sciences*, **92**(6), 1970–1974. https://doi.org/10.1073/pnas.92.6.1970

Howe, K., Bateman, A. and Durbin, R. (2002) QuickTree: building huge neighbour-joining trees of protein sequences. *Bioinformatics*, **18**(11), 1546–1547. https://doi.org/10.1093/bioinformatics/18.11.1546

Imazawa, R., Takahashi, Y., Aoki, W., Sano, M. and Ito, M. (2016) A novel type bacterial flagellar motor that can use divalent cations as a coupling ion. *Scientific Reports*, **6**(1), 19773. https://doi.org/10.1038/srep19773

Inoue, Y., Lo, C.-J., Fukuoka, H., Takahashi, H., Sowa, Y., Pilizota, T., *et al*. (2008) Torque-speed relationships of Na+-driven chimeric flagellar motors in *Escherichia coli*. *Journal of Molecular Biology*, **376**(5), 1251–1259. https://doi.org/10.1016/j.jmb.2007.12.023

Ives, A.R. and Garland, T. Jr. (2010) Phylogenetic logistic regression for binary dependent variables. *Systematic Biology*, **59**, 9–26.

Jaques, S., Kim, Y.K. and McCarter, L.L. (1999) Mutations conferring resistance to phenamil and amiloride, inhibitors of sodium-driven motility of *Vibrio parahaemolyticus*. *Proceedings of the National Academy of Sciences of the United States of America*, **96**(10), 5740–5745.

Kojima, S. and Blair, D.F. (2001) Conformational change in the stator of the bacterial flagellar motor. *Biochemistry*, **40**(43), 13041–13050. https://doi.org/10.1021/bi011263o

Kojima, S., Atsumi, T., Muramoto, K., Kudo, S., Kawagishi, I. and Homma, M. (1997) *Vibrio Alginolyticus* mutants resistant to phenamil, a specific inhibitor of the sodium-driven flagellar motor. *Journal of Molecular Biology*, **265**(3), 310–318. https://doi.org/10.1006/jmbi.1996.0732

Kojima, S., Asai, Y., Atsumi, T., Kawagishi, I. and Homma, M. (1999) Na+-driven flagellar motor resistant to phenamil, an amiloride analog, caused by mutations in putative channel components. *Journal of Molecular Biology*, **285**(4), 1537–1547. https://doi.org/10.1006/jmbi.1998.2377

Kojima, S., Furukawa, Y., Matsunami, H., Minamino, T. and Namba, K. (2008) Characterization of the periplasmic domain of MotB and implications for its role in the stator assembly of the bacterial flagellar motor. *Journal of Bacteriology*, **190**(9), 3314–3322. https://doi.org/10.1128/JB.01710-07

Kojima, S., Imada, K., Sakuma, M., Sudo, Y., Kojima, C., Minamino, T., *et al.* (2009) Stator assembly and activation mechanism of the flagellar motor by the periplasmic region of MotB. *Molecular Microbiology*, **73**(4), 710–718. https://doi.org/10.1111/j.1365-2958.2009.06802.x

Kojima, S., Takao, M., Almira, G., Kawahara, I., Sakuma, M., Homma, M., *et al*. (2018) The helix rearrangement in the periplasmic domain of the flagellar stator B subunit activates peptidoglycan binding and ion influx. *Structure*, **26**(4), 590–598.e5. https://doi.org/10.1016/j.str.2018.02.016

Koonin, E.V. (2016) Horizontal gene transfer: essentiality and evolvability in prokaryotes, and roles in evolutionary transitions. *F1000Research* **5**, 1805. https://doi.org/10.12688/f1000research.8737.1

Kuwajima, G. (1988) Construction of a minimum-size functional flagellin of *Escherichia coli*. *Journal of Bacteriology*, **170**(7), 3305–3309.

Larkin, M.A., Blackshields, G., Brown, N.P., Chenna, R., McGettigan, P.A., McWilliam, H., *et al*. (2007) Clustal W and Clustal X Version 2.0. *Bioinformatics*, **23**(21), 2947–2948. https://doi.org/10.1093/bioinformatics/btm404

Lo, C.-J., Sowa, Y., Pilizota, T. and Berry, R.M. (2013) Mechanism and kinetics of a sodium-driven bacterial flagellar motor. *Proceedings of the National Academy of Sciences*, **110**(28), E2544–E2551. https://doi.org/10.1073/pnas.1301664110

Maddison, W.P. and Maddison, D.P. (2015) Mesquite: A Modular System for Evolutionary Analysis. Version 3.04. https://www.mesquiteproject.org/.

Minamino, T., Terahara, N., Kojima, S. and Namba, K. (2018) Autonomous control mechanism of stator assembly in the bacterial flagellar motor in response to changes in the environment. *Molecular Microbiology*, **109**(6), 723–734. https://doi.org/10.1111/mmi.14092

Pallen, M.J. and Matzke, N.J. (2006) From the origin of species to the origin of bacterial flagella. *Nature Reviews Microbiology*, **4**(10), 784–790. https://doi.org/10.1038/nrmicro1493

Paulick, A., Delalez, N.J., Brenzinger, S., Steel, B.C., Berry, R.M., Armitage, J.P., *et al*. (2015) Dual stator dynamics in the *Shewanella oneidensis* MR-1 flagellar motor. *Molecular Microbiology*, **96**(5), 993–1001. https://doi.org/10.1111/mmi.12984

Rambaut, A. (2018) *FigTree v1.4.4, a Graphical Viewer of Phylogenetic Trees. 2014*. Java. https://github.com/rambaut/figtree.

Rossmann, F.M. and Beeby, M. (2018) Insights into the evolution of bacterial flagellar motors from high-throughput in situ electron cryotomography and subtomogram averaging. *Acta Crystallographica Section D: Structural Biology*, **74**(6), 585–594. https://doi.org/10.1107/S2059798318007945

Roujeinikova, A. (2008) Crystal structure of the cell wall anchor domain of MotB, a stator component of the bacterial flagellar motor: implications for peptidoglycan recognition. *Proceedings of the National Academy of Sciences*, **105**(30), 10348–10353. https://doi.org/10.1073/pnas.0803039105

Sharp, L.L., Zhou, J. and Blair, D.F. (1995) Tryptophan-scanning mutagenesis of MotB, an integral membrane protein essential for flagellar rotation in *Escherichia coli*. *Biochemistry*, **34**(28), 9166–9171. https://doi.org/10.1021/bi00028a028

Shih, P.M. and Matzke, N.J. (2013) Primary endosymbiosis events date to the later proterozoic with cross-calibrated phylogenetic dating of duplicated ATPase proteins. *Proceedings of the National Academy of Sciences*, **110**(30), 12355–12360. https://doi.org/10.1073/pnas.1305813110

Sowa, Y. and Berry, R.M. (2008) Bacterial flagellar motor. *Quarterly Reviews of Biophysics*, **41**(2), 103–132. https://doi.org/10.1017/S0033583508004691

Sowa, Y., Rowe, A.D., Leake, M.C., Yakushi, T., Homma, M., Ishijima, A. and Berry, R.M. (2005) Direct observation of steps in rotation of the bacterial flagellar motor. *Nature*, **437**(7060), 916–919. https://doi.org/10.1038/nature04003

Sugiyama, S., Cragoe, E.J. and Imae, Y. (1988) Amiloride, a specific inhibitor for the Na+-driven flagellar motors of alkalophilic bacillus. *The Journal of Biological Chemistry*, **263**(17), 8215–8219.

Terashima, H., Kawamoto, A., Morimoto, Y.V., Imada, K. and Minamino, T. (2017) Structural differences in the bacterial flagellar motor among bacterial species. *Biophysics and Physicobiology*, **14**, 191–198. https://doi.org/10.2142/biophysico.14.0_191

Terauchi, T., Terashima, H., Kojima, S. and Homma, M. (2011) A conserved residue, PomB-F22, in the transmembrane segment of the flagellar stator complex, has a critical role in conducting ions and generating torque. *Microbiology*, **157**(8), 2422–2432. https://doi.org/10.1099/mic.0.048488-0

Uyeda, J.C., Zenil-Ferguson, R. and Pennell, M.W. (2018) Rethinking phylogenetic comparative methods. *Systematic Biology*, **67**(6), 1091–1109. https://doi.org/10.1093/sysbio/syy031

Wilson, D.S. and Keefe, A.D. (2000) Random Mutagenesis by PCR. *Current Protocols in Molecular Biology*, **51**, 8.3.1–8.3.9.

Yakushi, T., Yang, J., Fukuoka, H., Homma, M. and Blair, D.F. (2006) Roles of charged residues of rotor and stator in flagellar rotation: comparative study using H+-driven and Na+-driven motors in *Escherichia coli*. *Journal of Bacteriology*, **188**(4), 1466–1472. https://doi.org/10.1128/JB.188.4.1466-1472.2006

Yakushi, T., Kojima, M. and Homma, M. (2004) Isolation of *Vibrio alginolyticus* sodium-driven flagellar motor complex composed of PomA and PomB Łdots. *Microbiology*. http://mic.sgmjournals.org/cgi/content/abstract/150/4/911.

Yonekura, K., Maki-Yonekura, S. and Homma, M. (2011) Structure of the flagellar motor protein complex PomAB: Implications for the torque-generating conformation. *Journal of Bacteriology*, **193**(15), 3863–3870. https://doi.org/10.1128/JB.05021-11

Yorimitsu, T. and Homma, M. (2001) Na+-driven flagellar motor of vibrio. *Biochimica et Biophysica Acta (BBA) - Bioenergetics* **1505**(1), 82–93. https://doi.org/10.1016/S0005-2728(00)00279-6

Yoshida, S., Sugiyama, S., Hojo, Y., Tokuda, H. and Imae, Y. (1990) Intracellular Na+ kinetically interferes with the rotation of the Na(+)-driven flagellar motors of *Vibrio alginolyticus*. *The Journal of Biological Chemistry*, **265**(33), 20346–20350.

Zhu, S., Takao, M., Li, N., Sakuma, M., Nishino, Y., Homma, M., *et al*. (2014) Conformational change in the periplamic region of the flagellar stator coupled with the assembly around the rotor. *Proceedings of the National Academy of Sciences* **111**(37), 13523–13528. https://doi.org/10.1073/pnas.1324201111

Supporting Information

Additional supporting information may be found online in the Supporting Information section at the end of the article